TECHNISCHE MECHANIK
European Journal of Engineering Mechanics
Diamond Open Access
journal homepage: www.ovgu.de/techmech

Tech. Mech., Vol. 46, Is. 1, (2026), 33–42
Received: 01.11.2025
Accepted: 08.01.2026
Available online: 16.02.2026

Development of a cylindrical-blade wind turbine driven by a necklace vortex

Tsutomu Takahashi[1]*, Ryuga Sadaoka[2], and Yasunori Sato[1],

[1] Nagaoka University of Technology, Department of Mechanical Mechanics, Faculty of Engineering, 1603-1 Kamitomioka, Nagaoka, Niigata. 940-2188 Japan
[2] Graduate School of Nagaoka University of Technology, Department of Mechanical Mechanics, 1603-1 Kamitomioka, Nagaoka, Niigata. 940-2188 Japan

Abstract: When the blade of a horizontal-axis wind turbine is replaced with a circular cylinder and a ring plate is installed downstream, a necklace vortex forms at their intersection. As the cylinder rotates, this vortex remains stationary on the opposite side of its motion, generating lift and driving the turbine. This is known as a necklace vortex-driven cylinder-blade wind turbine. Developed by the authors, this turbine rotates at less than 1/20th of the peripheral speed of conventional blade-type turbines while generating over ten times the torque. Its low speed eliminates noise and vibration, and the soft-material cylinder blades enhance safety, making it suitable for installation near human living spaces. The turbine consists of a single cylinder as the blade and a ring plate positioned in its wake. Key design parameters include the cylinder diameter and length, the diameter of the ring plate and radial width, and their spacing. This presentation examines how these factors influence power characteristics.

Keywords: cylindrical blade, horizontal axis wind turbine, necklace vortex, vertical vortex

Nomenclature

$C_{p\ max}/N$	[-] maximum power coefficient per blade
C_p	[-] power coefficient
$F_{L\ max}/N$	[N] lift force on cylinder blades
F_L	[N] lift force on cylinder blades
T_{max}/N	[Nm] maximum torque per blade
D	[mm] diameter of ring plate
d	[mm] diameter of cylinder blade
dW	[mm^2] product of d and W, that is effective lift-acting area of cylinder blade
L	[mm] length of cylinder blade
N	[-] number of blades
n	[rpm] rotational speed of blades
s	[mm] gap between blade and ring plate
s/d	[-] dimensionless gap normalized by blade diameter
T	[Nm] Torque acting on rotating shaft
U	[m/s] wind velocity
W	[mm] width of ring plate
W/d	[-] dimensionless ring width normalized by blade diameter

1 Introduction

Wind turbines used for wind power generation can be broadly classified into horizontal-axis wind turbines (HAWTs) and vertical-axis wind turbines (VAWTs) according to the orientation of the rotation axis (Hansen and Aagaard Madsen, 2011; Kumar et al., 2018). HAWTs can achieve high energy conversion efficiency because airfoil-shaped blades generate lift effectively (Hansen et al., 2006; Kassa et al., 2024), and therefore they have become the dominant technology for utility-scale wind power. However, HAWTs are inherently high-rotational-speed and low-torque machines, and noise and vibration issues, originating from blade aerodynamics as well as drivetrain components such as gearboxes and towers, tend to become pronounced (Hansen and Hansen, 2020; Zuo et al., 2020). In particular, their deployment in urban or residential areas is often constrained by environmental noise and safety considerations (Ahmed et al., 2025). In addition, yaw control to align the rotor with the incoming wind and pitch control to avoid

* E-mail address: ttaka@nagaokaut.ac.jp
doi: 10.24352/UB.OVGU-2026-005

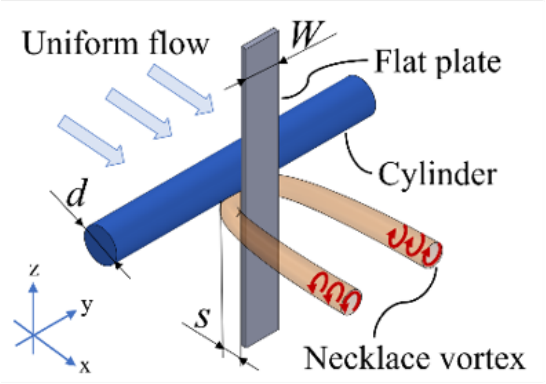

Fig. 1: Longitudinal vortices at cross-section of cruciform system with cylinder and flat plate.

stall are generally required, which increases the complexity of the mechanical structure and control system and may also raise maintenance and reliability concerns (Hansen and Aagaard Madsen, 2011; Kassa et al., 2024).

In contrast, VAWTs rotate about a vertical axis and can accept wind from any direction. As a result, they do not require a yaw mechanism and may offer a relatively simple configuration and improved adaptability to highly unsteady and turbulent inflow conditions (Kumar et al., 2018; Didane et al., 2024; Liu et al., 2019). Moreover, since major components such as generators and gearboxes can be located closer to the ground, VAWTs can provide advantages in maintainability; together with the possibility of operating at lower tip-speed ratios, they have been widely discussed for urban and distributed-generation applications (Kumar et al., 2018; Liu et al., 2019). Nevertheless, lift-driven Darrieus-type VAWTs typically suffer from poor self-starting capability and are prone to pronounced unsteady aerodynamics, including dynamic stall, due to the periodic variation of the angle of attack over one revolution (Didane et al., 2024; Abdolahifar and Zanj, 2025; Rathore et al., 2021). Drag-driven Savonius-type VAWTs exhibit favorable starting torque and are suitable for low-wind-speed and high-turbulence environments (Dewan et al., 2021; Chitura et al., 2024); however, they inherently show significantly lower power coefficients than lift-based designs (Dewan et al., 2021; Chitura et al., 2024). Furthermore, for many VAWTs, large cyclic variations in torque and aerodynamic loads within each revolution have been identified, leading to increased fatigue loading and reduced durability, which is regarded as one of the major barriers to commercialization (Didane et al., 2024; Liu et al., 2019; Abdolahifar and Zanj, 2025). Hence, although VAWTs offer practical merits in terms of configuration and operation, achieving both high efficiency and high reliability remains challenging.

As summarized above, neither conventional HAWTs nor VAWTs can be considered to fully satisfy the performance and social acceptance requirements for small-scale deployment in low-wind-speed urban environments (Kassa et al., 2024; Kumar et al., 2018; Didane et al., 2024; Liu et al., 2019; Dewan et al., 2021). A common feature of these conventional turbines is their reliance on aerodynamic mechanisms that directly exploit lift or drag associated with airfoil characteristics, which makes them highly sensitive to flow separation, stall, and variations in the angle of attack (Hansen and Aagaard Madsen, 2011; Hansen et al., 2006; Didane et al., 2024; Abdolahifar and Zanj, 2025). In particular, in urban areas where buildings induce strong spatial and temporal fluctuations in wind direction and speed, achieving stable operation while simultaneously maintaining low noise and low vibration is difficult (Ahmed et al., 2025; Kumar et al., 2018; Liu et al., 2019). Against this background, there is a strong need for new wind turbine concepts that can deliver high torque at low rotational speeds, with a simple and maintainable structure, while meeting low-noise and high-safety requirements (Zuo et al., 2020; Kumar et al., 2018; Didane et al., 2024; Liu et al., 2019; Abdolahifar and Zanj, 2025; Chitura et al., 2024).

A cylindrical-blade wind turbine driven by longitudinal vortices, whose vortex axis is aligned with the streamwise direction, is one promising candidate. It is known that when a circular cylinder and a downstream plate are arranged in a cruciform configuration with a prescribed gap, longitudinal vortices, typically represented by a necklace vortex and trailing vortices, are generated (Takahashi et al., 1999). Related three-dimensional wake structures at the intersection of two circular cylinders in a cruciform arrangement, closely associated with the formation of longitudinal vortical structures such as necklace and trailing vortices, have also been investigated experimentally by Fox (Fox, 1991), and further visualized around the center of a cross of tubes by Fox (Fox, 1990). These vortices are alternately and periodically formed and dissipated on the upper and lower sides near the intersection (Kato et al., 2012; Koide et al., 2006, 2017). Figure 1 schematically shows the moment when a necklace vortex forms on the lower side of the cylinder. Furthermore, when the cylinder is translated in a direction parallel to the plate and perpendicular to the main flow, as shown in Fig. 2, the periodicity of the necklace vortex is disrupted, and the vortex becomes localized on one side of the cylinder. In this condition, a steady lift force is produced on the upstream face of the cylinder as a reaction to the suction flow induced by the longitudinal vortex (Sakamoto et al., 2021a). As shown in Fig. 3, replacing the downstream flat plate with a ring plate and converting the cylinder motion from translation to rotation cause the necklace vortex to remain stationary on the side opposite to the cylinder motion, resulting in a rotational force induced by steady lift (Hemsuwan et al., 2018a). A wind turbine that utilizes this vortex-induced steady lift as the driving force is referred to as a longitudinal-vortex-driven cylindrical-blade wind turbine, which represents a new turbine concept based on an operating principle fundamentally different from that of conventional wind turbines (Sakamoto et al., 2021b; Hemsuwan et al., 2018b).

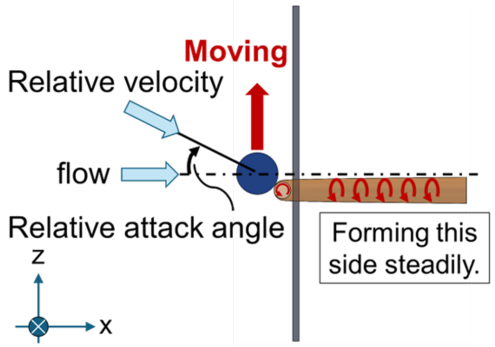

Fig. 2: Mechanism of lift force generation by Necklace vortex.

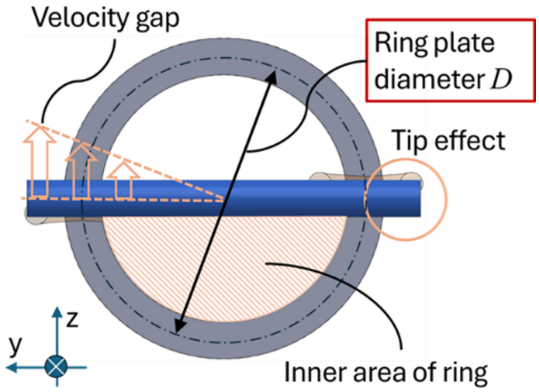

Fig. 3: Difference due to the curvature given to the flat plate.

Because the longitudinal-vortex-driven cylindrical-blade wind turbine can generate high torque at extremely low rotational speeds, it is expected to offer low noise, low vibration, and improved safety, making it suitable for small-scale, distributed, and near-urban wind power applications. On the other hand, to establish this turbine as a practical power generation system, it is essential to systematically clarify the effects of the key geometric parameters that govern both longitudinal vortex formation and turbine performance, and to formalize them as design guidelines. Indeed, it has been shown that the ring-plate width has a significant influence on turbine performance, and that there exists an optimal width-to-diameter ratio relative to the cylinder blade diameter (Sakamoto et al., 2021b).

Therefore, the objective of this study is to improve the power performance of a longitudinal-vortex-driven cylindrical-blade wind turbine and to systematically elucidate how the primary geometric parameters, namely the cylinder blade diameter, ring-plate width, and ring-plate center diameter, affect the turbine's power characteristics. In addition, by organizing the relationship between geometric constraints and power performance, this study aims to derive guidelines for selecting the optimal ring-plate geometry for any given cylinder blade diameter, and to propose a new performance index that enables turbine performance prediction based on representative geometric parameters. In this work, we focus on a single-cylinder-blade wind turbine, which has the simplest configuration, and evaluate its power characteristics through wind tunnel experiments in which the geometric parameters are systematically varied.

2 Experimental apparatus and methods

Figure 4a shows the platform used to evaluate the power characteristics of the longitudinal-vortex-driven cylindrical-blade wind turbine, and Fig. 4b presents a schematic definition of the representative geometric parameters. The platform allows the cylinder blade and the ring plate to be mounted, and the gap s between the cylinder blade and the ring plate can be adjusted to any desired value.

A rotary torque meter (UTMII-0.2 Nm, Unipulse Co., Ltd.) was connected to the rotation shaft to measure the torque and rotational speed simultaneously. In addition, an electromagnetic brake (HB0.5, OGURA CLUTCH Co., Ltd.) was installed at the most downstream end of the shaft. By applying a DC current to the brake, the load could be continuously varied, enabling measurements of the turbine power characteristics under controlled rotational-speed conditions. The measurement platform is placed inside the wind tunnel test section, allowing the power characteristics to be evaluated at arbitrary wind speeds.

As shown in Fig. 4b, the geometric parameters describing this turbine are the cylinder blade diameter d and length L, the average diameter D and width W of the ring plate, and the gap s between the cylinder blade and the ring plate. Moreover, since the turbine can be configured with multiple blades, the number of blades N is also treated as an important geometric parameter. Although these parameters can, in principle, be set independently, several geometric constraints exist in practice; for example, both ends of

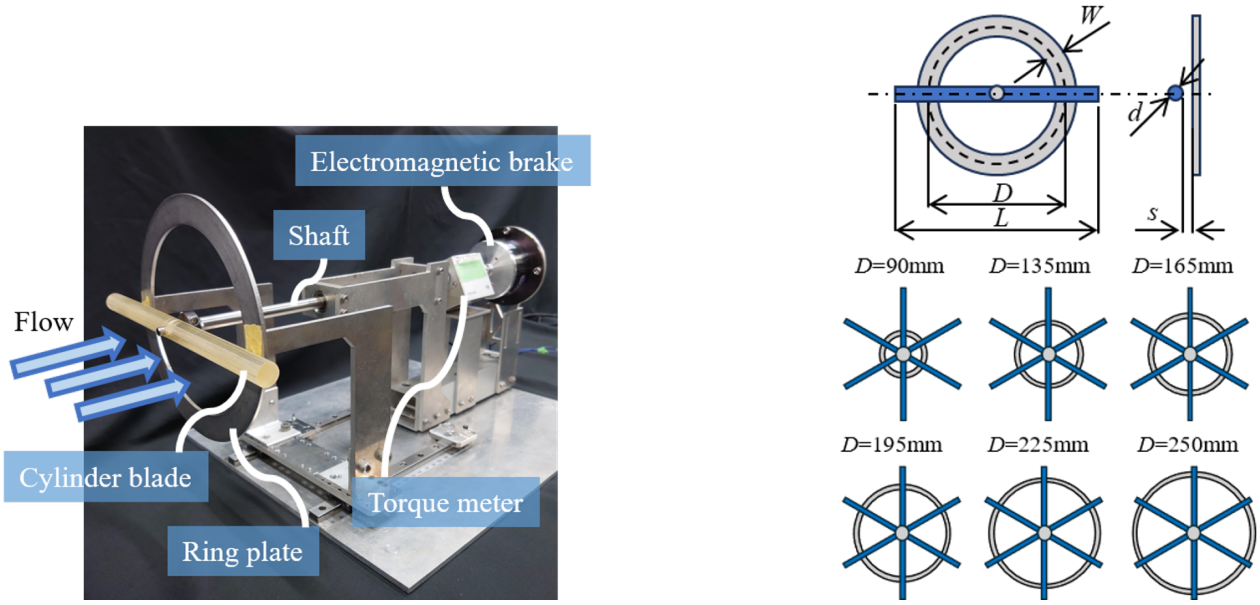

(a) Photograph of measurement platform (b) Representative geometric parameters

Fig. 4: Schematic of wind turbine device and each parameter.

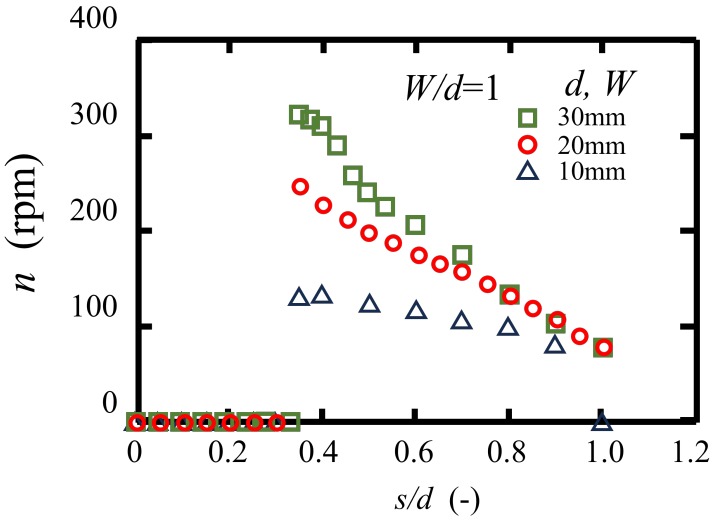

Fig. 5: Rotational speed as a function of normalized gap between cylinder and ring plate, where the gap is normalized by cylinder diameter ($W/d = 1$, $D = 155$mm, $L = 220$mm, $N = 2$, $U = 10$m/s).

the cylinder blade must protrude sufficiently beyond the ring plate. The power characteristics of the cylindrical-blade turbine are therefore determined by the interrelated effects of these geometric parameters.

Accordingly, to clarify the influence of the geometric parameters on the power characteristics experimentally, cylinder blades and ring plates of various sizes were fabricated, as listed in Table 1. Table 1 also summarizes the blade number N and the gap s used for each cylinder blade in the experiments. In this paper, the results obtained at a flow velocity of $U = 10$ m/s are presented. The cylinder length L was evaluated for three different values; however, the discussion focuses primarily on the results for $L = 280$ mm.

3 Results and discussion

3.1 Measured toque and evaluated lift force per blade

Figure 5 shows the measured relationship between the turbine rotational speed n and the normalized gap s/d, where the gap s between the cylindrical-blade and the ring plate is normalized by the cylinder diameter d. In this set of tests, the cylinder diameter d and the ring-plate width W were set to be identical (i.e., $W/d = 1$) in order to examine the effect of d ($= W$) on the $s/d - n$ relationship. Even with a constant W/d, the rotational speed increased as the cylinder blade and ring plate became thicker. In contrast, the s/d value that yields the maximum rotational speed was almost independent of d, indicating that the optimal condition lies in the range of $s/d = 0.3 - 0.4$. This result is in good agreement with the finding reported by (Sakamoto et al., 2021b) for a single-cylinder-blade turbine with $d = 20$ mm and $W = 20$ mm, where the optimal s/d was 0.35. When W/d was increased,

Tab. 1: Geometric parameters of the cylinder–ring plate configurations

Cylinder diameter d [mm]	Cylinder length L [mm]	Gap s [mm]	Number of blades N	Width of ring plate W [mm]	Average diameter of ring plate D [mm]
10	220, 250, 280	4	2, 6	10	90, 120, 135, 150, 155, 165, 180, 195, 210, 225, 240, 250
10	220, 250, 280	4	2, 6	15	85, 115, 130, 145, 160, 175, 190, 205, 220, 235, 245
10	220, 250, 280	4	2, 6	20	110, 115, 140, 170, 185, 200, 215, 230, 240
15	220, 280	6	2, 4	15	85, 115, 130, 145, 155, 175, 190, 205, 220, 235, 245
15	220, 280	6	2, 4	20	110, 115, 140, 170, 185, 200, 215, 230, 240
15	220, 280	6	2, 4	22.5	77.5, 107.5, 137.5, 152.5, 167.5, 182.5, 197.5, 212.5, 227.5, 237.5
15	220, 280	6	2, 4	30	70, 100, 130, 145, 160, 175, 190, 205, 220, 230
20	220, 250, 280	7	2	20	110, 140, 155, 170, 185, 200, 215, 230, 240
20	220, 250, 280	7	2	30	70, 100, 130, 145, 160, 175, 190, 205, 220, 230
20	220, 250, 280	7	2	40	60, 90, 120, 135, 150, 165, 180, 195, 210, 220
30	220, 250, 280	12	2	40	60, 90, 120, 135, 150, 165, 180, 195, 210, 220
40	220, 250, 280	15	2	40	60, 90, 120, 135, 150, 165, 180, 195, 210, 220
40	220, 250, 280	15	2	50	140, 185, 200
40	220, 250, 280	15	2	60	130, 175, 190
40	220, 250, 280	15	2	80	155
50	280	21	2	70	155
50	280	21	2	80	155

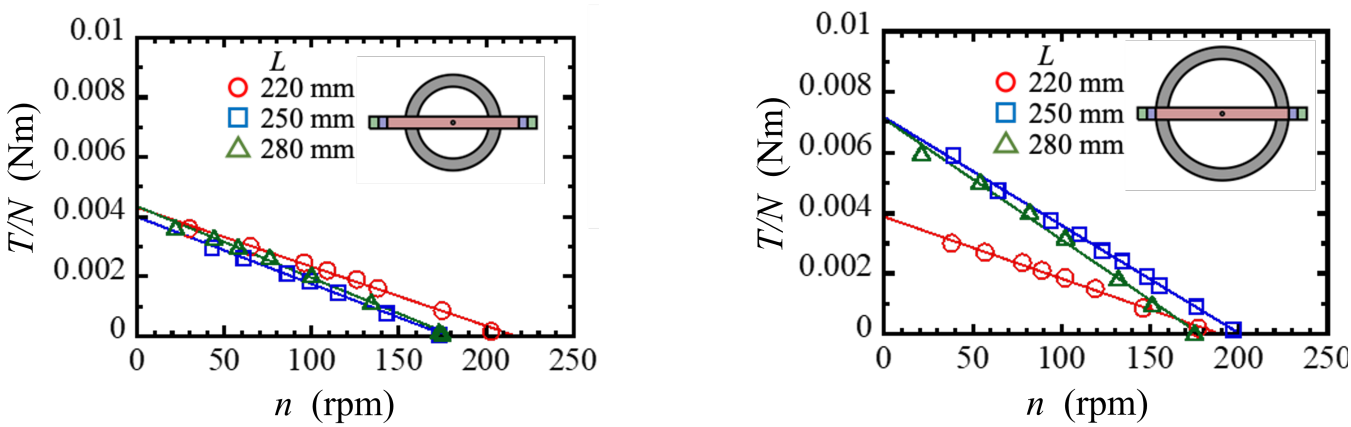

(a) D = 140 mm (b) D = 200 mm

Fig. 6: Relationship between rotational speed and torque per blade, defined as the total torque divided by the number of blades, for different cylinder lengths (d = 20 mm, W = 20 mm, s = 7 mm, N = 2, U = 10 m/s)

rotation was sometimes observed even at smaller s/d values (i.e., narrower gaps); however, stable rotation was generally obtained when s/d was approximately within 0.35-0.45. Based on these observations, in the subsequent experiments the gap s was fixed for each cylinder diameter d at the values listed in Table 1.

Figure 6 presents the torque per blade, T/N, measured while keeping the flow velocity and the geometrical conditions (cylindrical-blade, ring plate, and gap) constant, and reducing the rotational speed by applying a load to the shaft using the electromagnetic brake. As the rotational speed decreased under increasing load, the torque increased in an approximately linear manner. For D = 140 mm (Fig. 6a), the effect of the cylinder length L on the torque was small; however, for D = 200 mm (Fig.. 6b), the torque became smaller at L = 220 mm. At L = 220 mm, both ends of the cylinder blade coincide with the outer edge of the ring plate, and it is considered that the tip vortices, as illustrated schematically in Fig. 3, adversely affected the formation of the necklace vortex. Since the influence of L is not significant when both ends of the cylinder blade protrude sufficiently beyond the outer circumference of the ring plate, the subsequent experiments were conducted with L = 280 mm.

Figure 7 illustrates the influence of the average diameter of the ring-plate D on the torque and lift acting on the cylindrical-blade. As shown in Fig. 7a, the torque of this wind turbine increases almost linearly as the rotational speed decreases when a load is applied to the rotating shaft under a constant mainstream wind speed. Therefore, this torque curve was extrapolated using a linear approximation, and the maximum torque $T_{\max}$ was defined as the value obtained when the rotational speed reaches zero. Figure 7b illustrates the relationship between the diameter D of the ring plate and $T_{\max}$, while Figure 7c presents the relationship between the maximum steady lift force per blade $F_{L\,\max}/N$ and D, which was obtained by dividing $T_{\max}$ by D. Figure 7c indicates that

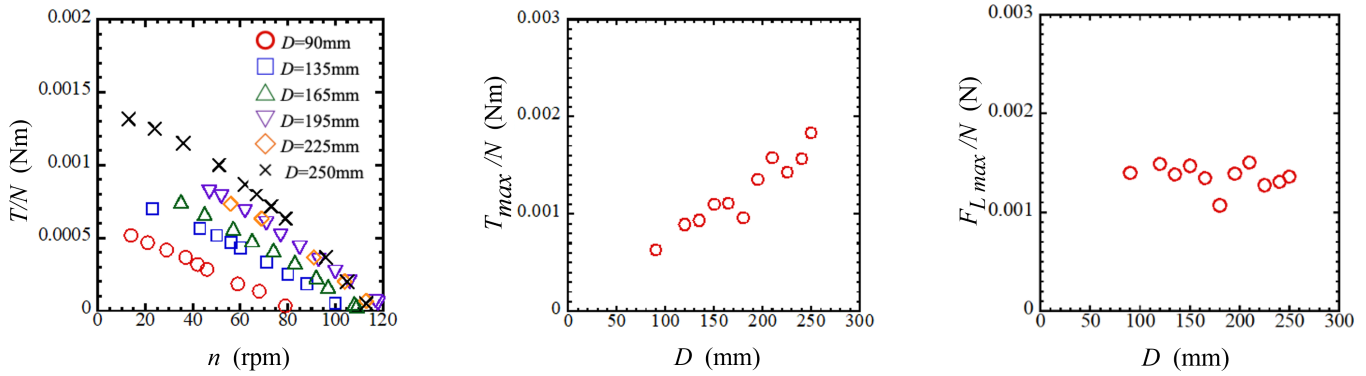

(a) Rotational speed vs. Torque

(b) Average diameter of ring-plate vs. Maximum torque

(c) Average diameter of ring-plate vs. Maximum lift force

Fig. 7: Effect of average diameter of ring plate D on measured torque and lift per blade (d = 10 mm, W = 10 mm, s = 4mm, L = 280 mm, N = 6, U = 10 m/s)

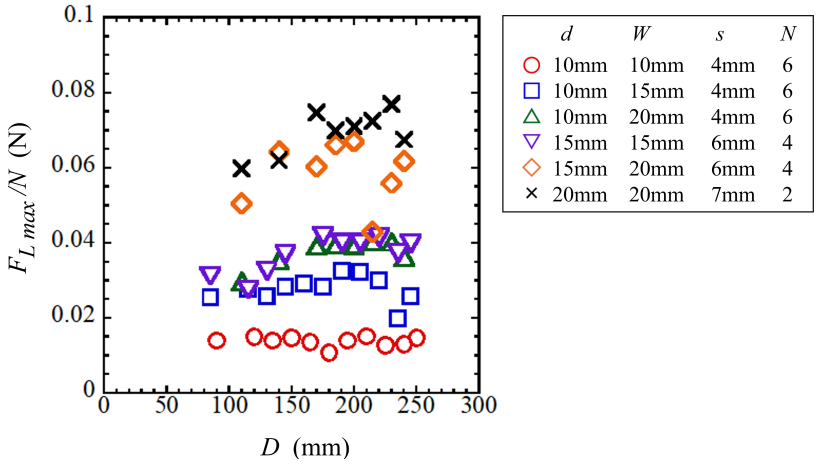

Fig. 8: Effect of ring plate diameter on maximum lift force for various cylinder diameters and ring plate widths (L = 280 mm, U = 10 m/s).

$F_{L\,\max}/N$ is nearly independent of D under these conditions.

This suggests that when the diameter of the cylindrical-blade d and ring width W are sufficiently small, the difference in radius of curvature or circumferential velocity between the inner and outer regions of the ring does not affect the lift, even as the ring diameter D decreases. Additionally, the effect of the vortex generated at the wingtip remains minimal, even if D increases and approaches the wingtip.

Figure 8 shows the maximum steady lift per blade, $F_{L\,\max}/N$, when D is varied for an arbitrary combination of d and W. For the d = 10 mm, W = 10 mm combination shown in Fig. 7c, $F_{L\,\max}/N$ remained approximately constant regardless of changes in D. However, for the d = 10 mm, W = 15–20 mm combinations, a decrease in $F_{L\,\max}/N$ was observed for both large and small values of D. When D is small, the difference in circumferential velocity between the inner and outer diameters of the ring becomes relatively large. Additionally, as D decreases, the size of the hub that supports the rotating shaft and blades remains unchanged, increasing the ratio of flow obstruction to the inner opening area of the ring. These factors contribute to the decrease in $F_{L\,\max}/N$ in the small D region.

3.2 Effective area of blade relative to lift

In a cylindrical-blade wind turbine driven by a necklace vortex, the lift is predominantly generated near the intersection between the cylindrical-blade and the ring plate. Therefore, increasing the blade diameter d and the ring width W is expected to enlarge the region where the vortex-induced suction acts, resulting in a larger lift force. To quantify this effect, a new parameter representing the lift-affected area dW is introduced, where dW represents d multiplied by W.

Figure 9a presents the maximum power coefficient per blade for various combinations of d (10-40 mm) and W (10-60 mm), obtained from the power-performance measurements. Over the entire parameter range, the power coefficient does not scale proportionally with dW, indicating that the turbine performance is influenced by additional factors that interfere with power generation. Figure 9b replots a subset of the data in Fig. 9a, restricted to cases where the normalized ring width satisfies $1 \leq W/d \leq 2$. Within this range, the maximum power coefficient shows an approximately proportional relationship with dW over a wide range of conditions. This

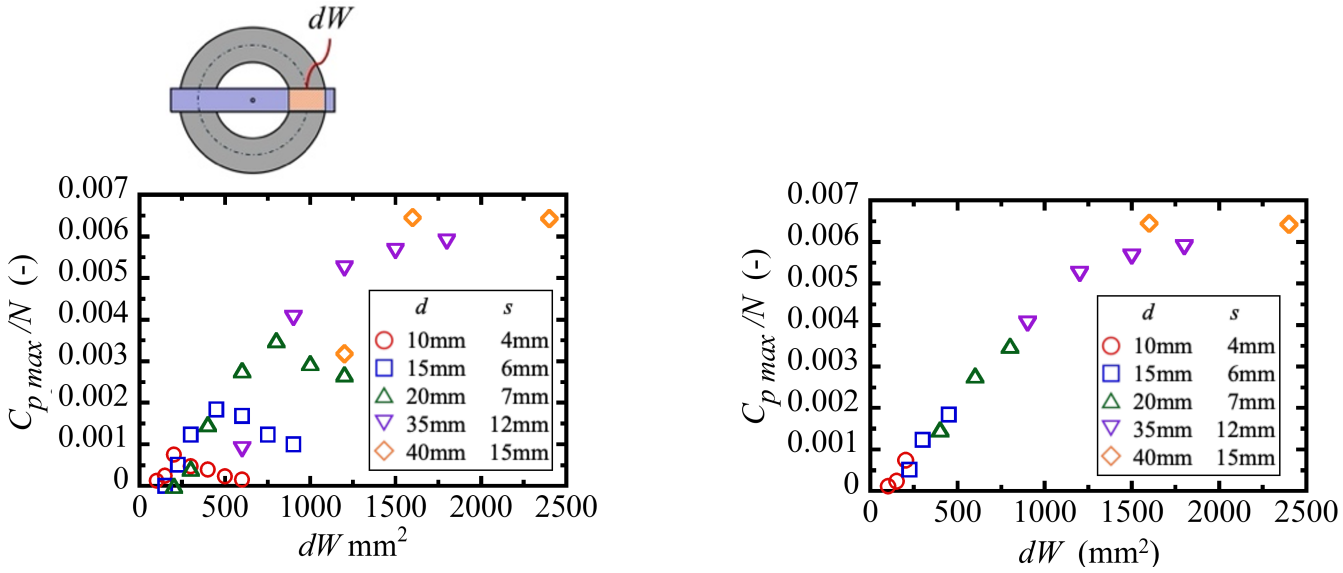

(a) Results for all d and W

(b) Results restricted to $1 \leq W/d \leq 2$

Fig. 9: Effect of effective area of blade dW on maximum power coefficient ($W = 10 - 60$ mm, $D = 155$ mm, $L = 220$ mm, $N = 2$, $U = 10$ m/s).

result suggests that designing the turbine with $1 \leq W/d \leq 2$ is effective for suppressing performance-degrading effects and for maintaining the expected scaling with the lift-affected area.

3.3 Geometric constraints for valid turbine configurations

A cylindrical-blade wind turbine is characterized by four primary geometric parameters: the blade diameter d, blade length L, the average diameter of the ring plate D, and the ring width W. These parameters are not fully independent because geometric constraints must be satisfied to ensure stable necklace-vortex formation and the resulting lift generation.

The first constraint is that the cylindrical blade must not obstruct the inner opening of the ring plate. Since the necklace vortex develops while wrapping around the ring in the width direction, a large d combined with a small D may partially block the opening and prevent stable vortex formation. When D denotes the average diameter of the ring plate, the inner diameter of the ring opening is given by $D - W$. Therefore, the following condition must be satisfied:

$$D - W > d. \tag{1}$$

Using the area parameter dW ($= d \times W$), this condition can be rewritten as

$$D > \frac{1}{d} dW + d. \tag{2}$$

The second constraint is that the blade must extend beyond the outer edge of the ring plate. If the blade length L is too short such that the blade tip remains inside the outer diameter of the ring, the necklace vortex cannot be formed. With D defined as the average diameter, the outer diameter of the ring plate is $D + W$. Hence, the blade length must satisfy

$$L > D + d. \tag{3}$$

Again, using dW ($= d \times W$), this condition can be expressed as

$$D < -\frac{1}{d} dW + L. \tag{4}$$

For turbine design, these two constraints are plotted on a plane with D on the vertical axis and dW on the horizontal axis, yielding the map shown in Fig. 10. A turbine configuration is geometrically feasible when its parameters fall within the triangular region bounded by Eq. 2 (magenta line) and Eq. 4 (green line). Figure 10 also presents representative turbine geometries located both inside and outside this feasible region.

3.4 Distribution of maximum lift force in *dW-D* map

Figure 11 plots the experimentally measured maximum lift for wind turbines with various geometries on the $dW - D$ map, where the color of each marker indicates the magnitude of the maximum lift coefficient. The two vertical blue lines correspond to $W/d = 1$ and $W/d = 2$. Turbines whose geometries lie outside the triangular region defined by Eqs. 2 and 4 exhibited little or no

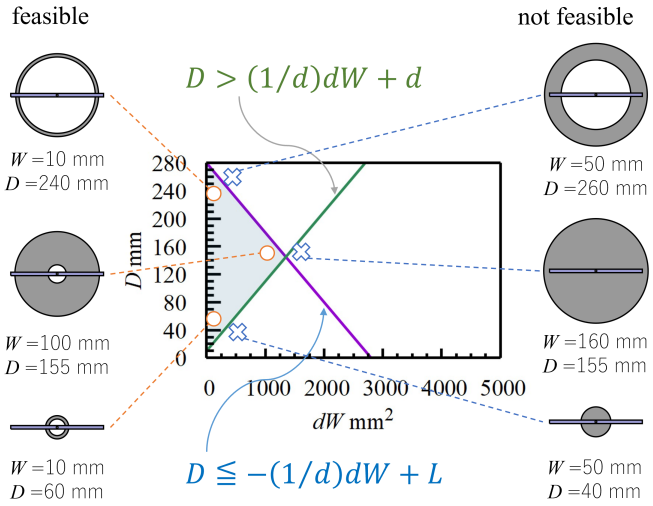

Fig. 10: Map illustrating the shape factors required for a cylindrical-blade wind turbine.

rotation. In contrast, within this triangular region—and particularly between the two blue lines—the cylindrical blades experienced a stable lift force. oreover, within this feasible region, larger values of dW tended to yield higher maximum power coefficients.

Figure 12 presents the same measurements on the $dW - D$ map for cases in which the cylinder diameter d was varied from 10 to 50 mm while the cylinder length L was fixed at 280 mm. The two vertic In this map, the effective geometric region is delineated by four boundary lines: Eqs. 2 and 4, together with the two lines corresponding to $W/d = 1$ and $W/d = 2$. As d increases, this feasible region shifts toward larger dW and expands. At the same time, the maximum lift acting on the cylindrical blades increases. These results indicate that the $dW - D$ map is a useful design tool: it visualizes the operable range of geometric parameters for this turbine and highlights the region in which improved performance can be expected.

4 Summary

This study investigated the power characteristics of a necklace-vortex-driven cylindrical-blade wind turbine, in which the steady lift induced by the necklace vortex acts as the driving force. The combined effects of the four primary geometric parameters, blade diameter d, blade length L, ring-plate average diameter D, and ring width W, were systematically examined. The results demonstrated that stable lift generation and effective power production are obtained when the normalized ring width satisfies $1 \leq W/d \leq 2$, and that the performance trends can be organized using the (dW, D) design map. In particular, turbine geometries located within the feasible triangular region defined by the geometric constraints (Eqs. 2 and 4) and between the W/d boundary lines exhibited stable operation, and larger dW generally led to higher maximum power coefficients. Based on these findings, a practical design guideline was established to select the ring-plate geometry that maximizes the maximum power coefficient for a given blade length.

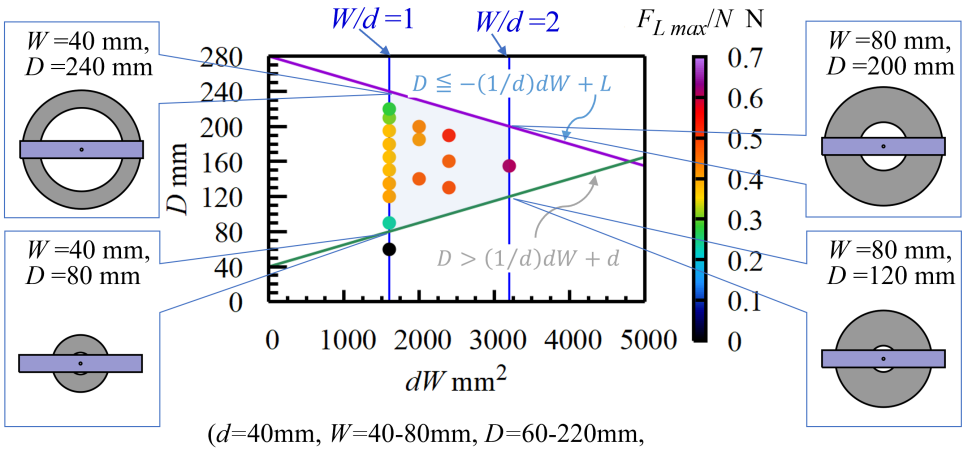

Fig. 11: Distribution of the maximum lift force on the $dW - D$ map.

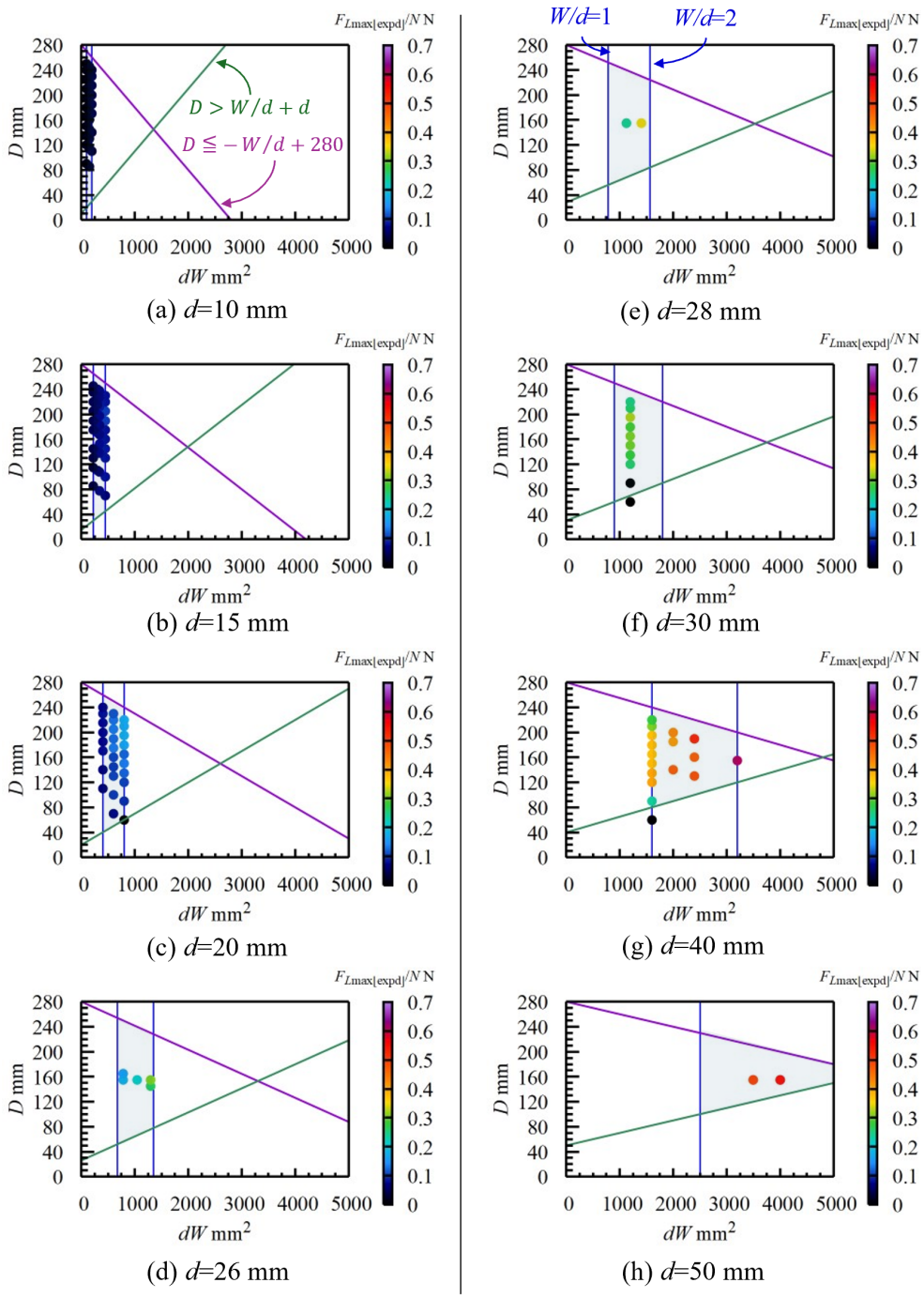

Fig. 12: Map of geometric conditions for effective operation of a circular cylindrical-blade wind turbine, including estimated maximum lift force and applicable constraints on W/d at $L = 280$ mm. Parameter ranges: $d = 10 - 50$ mm, $W = 10 - 80$ mm, $s = 4 - 21$ mm, $N = 2 - 6$, and $U = 10$ m/s.

References

A. Abdolahifar and A. Zanj. Development of a wind turbine driven by longitudinal vortex: Wind tunnel experiment to investigate the basic characteristics of the wind turbine. *Energy Conversion and Management*, 327:119575, 2025.

H.H. Ahmed, H.M. Robin, M.M.Z. Shahadat, and M.H. Masud. Innovative approaches for reducing wind turbine noise: A review from mechanical and aerodynamic perspective. *Energy Reports*, 13:728–746, 2025.

A.G. Chitura, P. Mukumba, and N. Lethole. Enhancing the performance of savonius wind turbines: A review of advances using multiple parameters. *Energies*, 17:3708, 2024.

A. Dewan, A. Gautam, and R. Goyal. Savonius wind turbines: A review of recent advances in design and performance enhancements. *Materials Today: Proceedings*, 47:2976–2983, 2021.

D.H. Didane, M.R. Behery, M. AI-Ghriybah, and B. Manshoor. Recent progress in design and performance analysis of vertical-axis wind turbines—a comprehensive review. *Processes*, 12:1094, 2024.

T.A. Fox. Flow visualization at the center of a cross composed of tubes. *International Journal of Heat and Flow*, 11:160–162, 1990.

T.A. Fox. Wake characteristics of two circular cylinders arranged perpendicularly to each other. *ASME Journal of Fluids Engineering*, 113:45–50, 1991.

C. Hansen and K. Hansen. Recent advances in wind turbine noise research. *Acoustics*, 2:171–206, 2020.

M.O.L. Hansen and H. Aagaard Madsen. Review paper on wind turbine aerodynamics. *Journal of Fluids Engineering*, 133: 114001, 2011.

M.O.L. Hansen, J.N. Sørensen, S. Voutsinas, N.N. Sørensen, and H. Aagaard Madsen. State of the art in wind turbine aerodynamics and aeroelasticity. *Progress in Aerospace Sciences*, 42:285–330, 2006.

W. Hemsuwan, K. Sakamoto, and T. Takahashi. Numerical investigation of lift-force generation on a moving circular cylinder in a uniform flow driven by longitudinal vortex. *Journal of Fluids and Structures*, 83:448–470, 2018a.

W. Hemsuwan, K. Sakamoto, and T. Takahashi. Lift force generation of a moving circular cylinder with a strip-plate set downstream in cruciform arrangement: Flow field improving using tip ends. *International Journals of Aeronautical and Space Sciences*, 19: 606–617, 2018b.

B.Y. Kassa, A.T. Baheta, and A. Beyene. Current trends and innovations in enhancing the aerodynamic performance of horizontal axis wind turbines: A review. *ASME Open Journal of Engineering*, 3:031001, 2024.

N. Kato, M. Koide, T. Takahashi, and M. Shirakashi. Vivs of a circular cylinder with a downstream strip-plate in cruciform arrangement. *Journal of Fluids and Structures*, 30:97–114, 2012.

M. Koide, K. Ootani, S. Yamada, T. Takahashi, and M. Shirakashi. Vortex excitation caused by longitudinal vortices shedding from cruciform cylinder system in water flow. *JSME International Journal Series B*, 49:1043–1048, 2006.

M. Koide, T. Takahashi, M. Shirakashi, and S.A.Z.B.S. Salim. Three-dimensional structure of longitudinal vortices shedding from cruciform two-cylinder systems with different geometries. *Journal of Visualization*, 20:753–763, 2017.

R. Kumar, K. Raahemifar, and A. S. Fung. A critical review of vertical axis wind turbines for urban applications. *Renewable and Sustainable Energy Reviews*, 89:281–291, 2018.

X. Liu, H. Lin, and J. Zhang. Review on the technical perspectives and commercial viability of vertical axis wind turbines. *Ocean Engineering*, 182:608–626, 2019.

M. K. Rathore, M. Agrawal, and P. Baredar. Pitch control mechanism in various type of vertical axis wind turbines: A review. *Journal of Vibration Engineering & Technologies*, 9:2133–2149, 2021.

K. Sakamoto, W. Hemsuwan, and T. Takahashi. Development of circular cylinder blade wind turbine driven by longitudinal vortex. *Transactions of the JSME (in Japanese)*, 87(894):20–00365, 2021a.

K. Sakamoto, W. Hemsuwan, and T. Takahashi. Development of a wind turbine driven by longitudinal vortex: Wind tunnel experiment to investigate the basic characteristics of the wind turbine using a single circular cylinder blade. *Journal of Wind Engineering and Industrial Aerodynamics*, 210:104492, 2021b.

T. Takahashi, L. Baranyi, and M. Shirakashi. Configuration and frequency of longitudinal vortices shedding from two cylinders in cruciform arrangement. *Journal of Visualization Society of Japan*, 19:328–336, 1999.

H. Zuo, K. Bi, and H. Hao. A state-of-the-art review on the vibration mitigation of wind turbines. *Renewable and Sustainable Energy Reviews*, 121:109710, 2020.